ChemPhysChem

Research Article
doi.org/10.1002/cphc.202300365

Chemistry Europe
European Chemical
Societies Publishing

www.chemphyschem.org

Electronic Structure of the Low-Lying States of the Triatomic MoS$_2$ Molecule: The Building Block of 2D MoS$_2$

Markella A. Mermigki,[a] Ioannis Karapetsas,[a] and Demeter Tzeli*[a, b]

Molybdenum disulfide (MoS$_2$) is the building component of 1D-monolayer, 2D-layered nanosheets and nanotubes having many applications in industry, and it is detected in various molecular systems observed in nature. Here, the electronic structure and the chemical bonding of sixteen low-lying states of the triatomic MoS$_2$ molecule are investigated, while the connection of the chemical bonding of the isolated MoS$_2$ molecule to the relevant 2D-MoS$_2$, is emphasized. The MoS$_2$ molecule is studied via DFT and multireference methodologies, i.e., MRCISD(+Q)/aug-cc-pVQZ(−PP)$_{Mo}$. The ground state, $\tilde{X}^3B_1$, is bent (Mo−S= 2.133 Å and φ(SMoS)=115.9°) with a dissociation energy to atomic products of 194.7 kcal/mol at MRCISD+Q. In the ground and in the first excited state a double bond is formed between Mo and each S atom, i.e., $a_1^2a_1^2b_2^2a_2^2$. These two states differ in which d electrons of Mo are unpaired. The Mo−S bond distances of the calculated states range from 2.108 to 2.505 Å, the SMoS angles range from 104.1 to 180.0°, and the Mo−S bonds are single or double. Potential energy curves and surfaces have been plotted for the $\tilde{X}^3B_1$, $^5A_1$ and $^5B_1$ states. Finally, the low-lying septet states of the triatomic molecule are involved in the material as a building block, explaining the variety of its morphologies.

Introduction

Molybdenum disulfide is the building component of 1D monolayer, 2D layered nanosheets and nanotubes having many applications in industry. It has been characterized as a high performance material with low cost due to its high earth reserves and its high catalytic activity.[1–8] Specifically, the materials or complexes of MoS$_2$ can be used as gas sensors for industrial affiliated gases,[9,10] catalysts,[11] photodetectors[12] and additionally have application in energy storage through their contribution in the construction of sodium ion batteries.[13] Finally, the molybdenum disulfide is also detected in molecular systems that are observed in nature, such as in the FeMo cofactor of nitrogenase which catalyzes the process of nitrogen fixation.[14]

Regarding MoS$_2$ material, many studies have been carried out and different means and strategies have been followed including the structural engineering, phase conversion, composition tuning, and the interlayer regulation method[3,15] to improve its catalytic properties. However, these studies have not yet been sufficient to meet the requirements for successful applications.[16] It is known that the physical and catalytic properties of a solid are influenced by the structural features.[17] Thus, it is important to study the intrinsic electronic structure of the MoS$_2$ unit as well as its bonding properties and its geometry. Data regarding this building block unit will be useful for the investigation of more complicated systems of Mo and S atoms. Additionally, it is important to investigate how the properties of the MoS$_2$ unit change depending on the surroundings. This knowledge could assist in improving the functionality of the complexes or material including MoS$_2$ units.

As far as we know, even though the study of the MoS$_2$ molecule is very important, there is only one joint experimental and theoretical study on the MoS$_2$ triatomic molecule,[18] and one study on its cation.[19] In 2002, the infrared spectrum of the MoS$_2$ molecule was measured.[18] Using resolved metal isotopic absorptions for MoS$_2$ and sulfur isotopic absorptions for the antisymmetric stretching mode, the S−Mo−S bond angle was determined as 114°±3°.[18] Additionally, via DFT methodology (B3LYP and BPW91/6-311+G*$_S$LANL2DZ$_{Mo}$) the geometry and the frequencies of three states, i.e., $^3B_1$, $^3A_1$ and $^1A_1$, were calculated.[18] Regarding the MoS$_2^+$ cation, its Gibbs formation energy is provided.[19] Specifically, the reaction of Mo$^+$ cation and 45 other atomic-metal cations with CS$_2$ have been investigated at room temperature via inductively-coupled plasma/selected-ion flow tube tandem mass spectrometry.[19]

Recently, we studied the diatomic MoS molecule both theoretically and experimentally, and emphasis was given to the formation of molybdenum-sulfur bond explaining the stability and the variety of the shapes and morphologies of the material.[20] As a continuation of this research, here we study the triatomic MoS$_2$, which is the exact building block unit of the MoS$_2$ 2D layers. In the present work, the ground and fifteen low-lying excited states of MoS$_2$ are studied via accurate multi reference configuration interaction methodologies. The chemical bonds connecting the atoms are analyzed, while potential energy curve (PEC) and potential energy surfaces are provided.

[a] M. A. Mermigki, Dr. I. Karapetsas, Prof.Dr. D. Tzeli
Laboratory of Physical Chemistry, Department of Chemistry, National and Kapodistrian University of Athens, Panepistimiopolis Zografou, Athens 157 84, Greece
E-mail: tzeli@chem.uoa.gr

[b] Prof.Dr. D. Tzeli
Theoretical and Physical Chemistry Institute, National Hellenic Research Foundation, 48 Vassileos Constantinou Ave, Athens 116 35, Greece

ChemPhysChem

Research Article
doi.org/10.1002/cphc.202300365

Chemistry Europe
European Chemical
Societies Publishing

Finally, the connection of the chemical bonding of the isolated MoS_2 molecule to the relevant solid, MoS_2, is emphasized to shed light on the functionality of the MoS_2 complexes or materials.

Computational Details

Fifteen low-lying electronic states of the MoS_2 molecule were calculated. At first, the lowest singlet, triplet, quintet and septet states of the MoS_2 molecule were calculated via density functional theory employing the TPSSh functional[21] in conjunction with the correlation consistent aug-cc-pVQZ[22] basis set for the S atoms $(17s,12p,4d,3f,2g) \rightarrow [7s,6p,4d,3f,2g]$, and the corresponding basis set including pseudopotential for the Mo atom, aug-cc-pVQZ-PP,[23] $(17s,14p,12d,5f,4g,3h,2i) \rightarrow [8s,8p,7d,5f,4g,3h,2i]$. The latter basis sets employ accurate core relativistic pseudo-potentials for the $1s^2 2s^2 2p^6 3s^2 3p^6$ electrons and treat the $4s^2 4p^6(5s4d)^6$ electrons of Mo in the ab initio calculation. The aug-cc-pVQZ$_S$ aug-cc-pVQZ-PP$_{Mo}$ (AVQZ-(PP)$_{Mo}$) basis set includes 473 primitive atomic orbitals which are reduced to 365 after the contraction.

Then, 16 low-lying electronic states, i.e., singlet, triplet, quintet, and septet states were calculated via multireference methodologies. The complete active space self-consistent field (CASSCF) method,[24] the multireference configuration interaction+single+double excitations (MRCISD)[25] and MRCISD+Q,[26] where the Davidson correction (+Q) was included in MRCISD, methodologies were used employing the aug-cc-pVQZ(−PP)$_{Mo}$ basis set. In the CASSCF approach, 14 valence electrons are allocated in 12 valence orbitals, i.e., the six $4d^5 5s^1$ electrons of the Mo atom and the four $3p^4$ electrons of S atoms. The $3s^2$ electrons of the S atoms were kept frozen in the CASSCF space to retain the molecular orbitals in the correct ordering in the CASSCF space. The number of configuration state functions (CSFs) ranges from 7504 for septet states to 70880 for the triplet states. Then all sixteen studied electronic states were calculated at the MRCISD level applying the internal contraction approximation (icMRCISD).[25] The number of MRCISD CSFs of singlet states are up to 5.8×10^9 and they are reduced to 2.5×10^7 after the ic approach. For the triplet states, the MRCISD CSFs are 11.3×10^9 and are reduced to 4.4×10^7 (ic), for the quintet states they are 7.7×10^9 and are reduced to 2.7×10^7 (ic), while for the septet states, are 2.7×10^9 and 8.8×10^6, respectively. The molecule has C_{2v} symmetry, and all calculations were carried out under the C_{2v} symmetry restrictions. Geometries (R, φ), dipole moments (μ),

frequencies (ω_e), and dissociation energies (D_e) were calculated. Three dissociation energies were calculated with respect to different dissociation products, i.e., $D_e^1 = -[E(MoS_2)-E(Mo)-2 \times E(S)]$, $D_e^2 = -[E(MoS_2)-E(MoS)-E(S)]$, and $D_e^3 = -[E(MoS_2)-E(Mo)-E(S_2)]$. The relative energies (T_e) were calculated with respect to the ground state of the molecule, $T_e = E-E(X)$. The chemical bonding of all states is analyzed, while for the low-lying states, MRCI potential energy curves (PECs) and potential energy surfaces (PESs) were plotted.

Finally, the 2D MoS_2 layer was studied via periodic DFT calculations using the generalized gradient approximation (GGA) with the Perdew–Burke–Ernzerhof (PBE)[27] functional to describe the electron exchange and correlation. The DFT-D3[28] method of dispersion correction was added which has been widely used for the MoS_2 systems and the projector augmented waves (PAW) pseudopotentials[29] JK-type were employed. The kinetic energy cutoff was 50 Ry. The energy and residual forces convergence criteria were set as 10^{-6} Ry and 10^{-5} Ry during structural optimization, respectively. A 6×6 layer supercell was built and a 6 Å vacuum layer was added to minimize the interactions between the TMDC monolayers and their images. The Gamma k-point was used for geometry relaxation. All atoms were fully relaxed without any constraint.

The DFT calculations on the triatomic MoS_2 molecules were carried out via Gaussian16,[30] the CASSCF and icMRSISD(+Q) calculations were carried out via Molpro2022.3,[31] while the periodic DFT calculations on the 2D MoS_2 material were carried out via the Quantum Espresso code.[32]

Results and Discussion

DFT Methodology

First, the lowest singlet, triplet, quintet, and septet states of MoS_2 were calculated at the TPSSh/AVQZ(−PP)$_{Mo}$ methodology, see Table 1. Additionally, two transition states, the $^5A_2$ state presenting one imaginary frequency in the antisymmetric vibrational mode and the linear $^5\Sigma_u$ state having imaginary frequencies in the two bending vibrational modes, showing that the molecule is bent. In all calculated electronic states, the

Table 1. Bond distances R (Mo−S and S−S) in Å, φ (S−Mo−S) in degrees, dissociation energy with respect to atomic ground states products D_e^1 in kcal/mol, expectation values of dipole moments μ in Debye, frequencies ω_e [a] in cm^{-1}, corresponding IR intensities, and energy differences T_e in kcal/mol at MRCISD(+Q)/AVQZ-PP levels of theory and energy differences T_e in kcal/mol at the TPSSh/AVQZ(−PP)$_{Mo}$ methodology.

State	R(Mo−S)	R(S−S)	φ (SMoS)	D_e^1	μ	$\omega_{e,b}$	IR	$\omega_{e,ss}$	IR	$\omega_{e,as}$	IR	T_e
$\tilde{X}^3B_1$	2.114	3.546	114.0	200.7	3.70	166.7	0.0118	541.0	9.767	549.8	111.32	0.00
[b]	2.132		113.5			165.6		523.8		534.8		
[c]	2.135		112.4			170.1		516.4		528.2		
Expt[d]			114±3							535.7		
$^1A_1$	2.090	3.371	107.5	184.9	4.20	187.9	1.211	563.9	99.667	563.0	14.088	15.73
$^5A_2$	2.178	3.955	130.4	166.3	1.33	43.76	4.820	438.6	22.032	254.5i	157.98	34.41
$^5A''$	2.128, 2.268	4.017	132.0	166.6	1.58	66.3	3.076	251.5[e]	13.466	508.4	19.661	34.06
$^5\Sigma_u$	2.163	4.327	180.0	164.9	0.00	52.4i^f	1.143	438.6	0.000	462.3	23.593	35.81
$^7B_1$	2.339	3.934	114.5	115.6	2.38	51.3	5.468	360.5	126.71	262.4	25.009	85.03

[a] $\omega_{e,b}$: bending mode (A_1 symmetry); $\omega_{e,ss}$: symmetric stretch (A_1 symmetry); $\omega_{e,as}$: antisymmetric stretch (B_2 symmetry). [b] Ref. [18]; B3LYP/6-311+G*$_S$LANL2DZ$_{Mo}$. [c] Ref. [18]; BPW91/6-311+G*$_S$LANL2DZ$_{Mo}$. [d] Ref. [18]. [e] Antisymmetric stretching.

ChemPhysChem

Research Article
doi.org/10.1002/cphc.202300365

**Chemistry
Europe**
European Chemical
Societies Publishing

Mo atom forms bonds with two S atoms and not with the S_2 molecule. The ground state of S_2 is the $X^3\Sigma_g^-$ state with a bond distance of 1.901 Å and a D_e value of 104.9 kcal/mol at TPSSh/AVQZ, while in all bent calculated states the S—S distance ranges from 3.371 Å ($^1A_1$) to 4.017 Å ($^5A''$). The ground state is the $\tilde{X}^3B_1$ state, with an R(Mo—S) bond distance of 2.114 Å and an S—Mo—S angle of 114.0 degrees. The last value is in excellent agreement with the experimental value of the S—Mo—S angle of 114 ± 3 degrees.[18] The dissociation energy with respect to the ground states of the atomic products is 200.7 kcal/mol. The dipole moment is 3.70 Debye, and the vibrational modes are 166.7 cm^{-1} for the bending motion, 541.0 cm^{-1} for the symmetric stretching and 549.8 cm^{-1} for the antisymmetric stretching. The calculated antisymmetric vibrational mode is in very good agreement with the experimental value of 535.7 cm^{-1}.[18]

The DFT population analysis of the ground state was performed within the Mulliken, natural population analysis (NPA), Hirshfeld (H) and its charge model 5 (CM5) framework, using the VTZ($-$PP)$_{Mo}$ and AVQZ($-$PP)$_{Mo}$ to test the basis set dependance. The Hirshfeld, CM5 and NPA charges are basis set independent, i.e., the charges on Mo for the above basis sets are q$_{Mo}$: $+0.48$ and $+0.49$ (Hirshfeld), $+0.78$ and $+0.78$ (CM5), $+0.31$ and $+0.34$ (NPA). On the contrary, the Mulliken analysis present huge difference, i.e., $+0.12$ e$^-$ using the triplet-ζ basis set and -1.11 e$^-$ using the augmented basis set. It is well-known that Mulliken charges can show basis set dependency[33–34] or underestimation of the ionic character and it is advised to be used with rather small non augmented basis sets.[35] The NPA method is regarded as an improved alternative to the extensively used Mulliken population,[36–37] but NPA can overestimate the ionic character of the atoms.[37] In the present study, it was found that the CM5 analysis presents the largest calculated charges on Mo. Hirshfeld predicts charges smaller than CM5, but they are larger than the NPA charges. Additional calculations with M06 DFT functional, gives the same charges for each analysis. Generally, it is agreed that the use of the population analyses is indicative and helps to make comparisons among similar molecular systems, structures, or states.[33–36] Here, it is regarded the NPA charges as the most accurate ones,[33–36] i.e., the charge of the Mo atom is about $+0.3$ e$^-$.

The septet state, $^7B_1$, was calculated at 85.0 kcal/mol above the ground state at TPSSh. In $^7B_1$, the Mo atom forms one bond with each S atom, while in the ground state the Mo forms two bonds with each S atom, see Scheme 1 and discussion below. Comparing the $\tilde{X}^3B_1$ state with the $^7B_1$ state, the change from a double Mo—S bond in the triplet state to a single Mo—S bond in the septet state, results to an increase of the Mo—S distance by 0.2 Å, while the SMoS angle value remains the same in both states. Furthermore, the dipole moment is decreased by 1.4 Debye, while the dissociation energy is decreased by 42%, see Table 1.
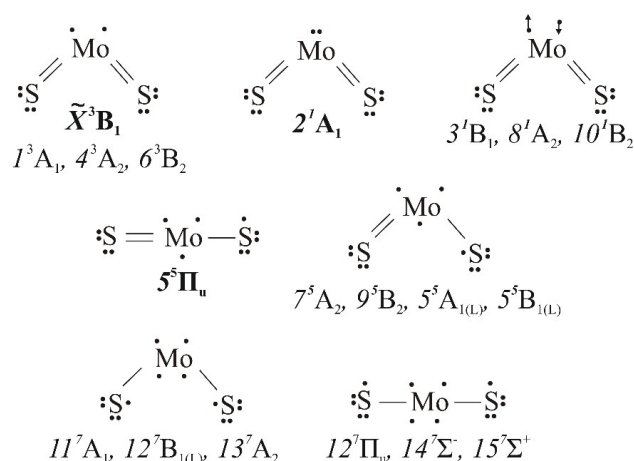
Scheme 1. Chemical bonding of the calculated states.

Multireference Methodology

Sixteen low-lying electronic states were calculated via multi-reference methodologies, i.e., CASSCF, icMRCISD($+$Q)/AVQZ-PP$_{Mo}$. The geometries, the dissociation energies, dipole moments, and energy differences are presented in Table 2. In all sixteen calculated electronic states, the Mo atom forms single or multiple bonds with each of the two S atoms and not with the S_2 molecule. In all bent calculated states, the S—S distance ranges from 3.390 Å ($^1A_2$) to 4.325 Å ($^5B_2$) at the icMRCISD$+$Q, see Table 2. The main electronic Configuration State Functions (CSF) of the calculated states are given in Table 3. Given that the augmentation of the basis set results in wrong Mulliken charges, see above, the population analysis was obtained using the cc-pVTZ($-$PP) basis set. For the ground state, the calculated CASSCF Mulliken charge on Mo is $+0.26$ and the corresponding CASSCF NPA charge is $+0.31$. In all states, the Mo is positively charged, see Table 4, as it is expected given that Pauling electronegativities is largest for the S atom, i.e., they are 2.16 (Mo) and 2.58 (S). The dipole moment is along the C_2 axis and it is pointing from metal to S according to the convention in chemistry. Finally, potential energy curves (PECs) and potential energy surfaces (PESs) and plots of dipole moments with respect to geometry are depicted in Figures 1–6.

Ground State, $\tilde{X}^3B_1$

In the ground state, $\tilde{X}^3B_1$, the Mo—S bond distances are calculated at 2.133 Å and the SMoS angle at 115.9° in very good agreement with the experimental value of 114 ± 3 degrees.[18] The PEC of the ground state keeping the SMoS angle at 115.9° and pulling the S atoms symmetrically apart with respect to the Mo—S distance is depicted in Figure 1. The dissociation energy of the X state with respect to Mo (^7S) $+$ 2S (^3P), D_e^1, is calculated at 194.7 kcal/mol at the icMRCISD$+$Q level of theory.

The dissociation energy D_e^2 with respect to the antisymmetric pulling of the one S atom, where the X state dissociates to MoS ($X^5\Pi$) $+$ S (^3P) is 108.8 kcal/mol, while the dissociation

ChemPhysChem

Research Article
doi.org/10.1002/cphc.202300365

Chemistry Europe
European Chemical
Societies Publishing

Table 2. Bond distances R (Mo—S and S—S) in Å, φ (S—Mo—S) in degrees, dissociation energy D_e[a] in kcal/mol, expectation values of dipole moments μ in Debye and energy differences T_e in kcal/mol at the CASSCF, icMRCISD(+Q)/ AVQZ(−PP)$_{Mo}$ methodologies.

State	Methods	R (Mo—S)	R (S—S)	φ (SMoS)	D_e^{1}[a]	D_e^{2}[a]	D_e^{3}[a]	μ	T_e
$\tilde{X}^3B_1$	CAS	2.1594	3.703	118.1	137.4	87.7	58.9	4.28	0.00
	icMRCISD	2.1334	3.617	115.9	185.3[b]	100.6	78.9	4.10	0.00
	icMRCISD+Q				194.7[b]	108.8	90.5		0.00
Expt[c]				114±3					
1^3A_1	CAS	2.1617	3.704	117.9	129.2	79.5	50.7	2.39	8.24
	icMRCISD	2.1398	3.654	117.3	165.4	90.0	68.3	2.33	10.63
	icMRCISD+Q				181.9	97.6	79.3		11.21
2^1A_1	CAS	2.1285	3.494	110.3	125.4	75.7	46.9	4.78	12.01
	icMRCISD	2.1085	3.421	108.4	163.5	88.0	66.4	4.53	12.57
	icMRCISD+Q				180.0	95.7	77.3		13.17
3^1B_1	CAS	2.1539	3.692	118.0	114.6	64.9	36.1	4.61	22.80
	icMRCISD	2.1285	3.593	115.1	155.7	80.3	58.6	4.42	20.30
	icMRCISD+Q				173.4	89.1	70.8		19.76
4^3A_2	CAS	2.1903	3.480	105.2	110.8	61.1	32.3	5.83	26.66
	icMRCISD	2.1618	3.412	104.2	148.8	73.4	51.7	5.63	27.20
	icMRCISD+Q				165.8	81.5	63.1		27.38
$5^5\Pi_u$[d]	CAS	2.2920	4.584	180.0	105.7	56.0	27.2	0.00	31.69
	icMRCISD	2.2574	4.515	180.0	139.5	64.1	42.4	0.08	36.53
	icMRCISD+Q				155.6	71.3	53.0		37.49
6^3B_2	CAS	2.2015	3.634	111.3	97.1	47.4	18.6	5.77	40.34
	icMRCISD	2.1714	3.560	110.1	137.0	61.6	39.9	5.54	39.03
	icMRCISD+Q				154.9	70.6	52.3		38.19
7^5A_2	CAS	2.2425	4.106	132.5	101.5	51.8	23.0	1.64	35.90
	icMRCISD	2.2078	3.912	124.8	136.9	61.5	39.8	1.78	39.08
	icMRCISD+Q				154.3	70.0	51.7		38.86
8^1A_2	CAS	2.1742	3.449	105.0	94.4	44.7	15.9	5.48	43.04
	icMRCISD	2.1493	3.39	104.1	134.9	59.5	37.8	5.28	41.07
	icMRCISD+Q				152.3	68.1	49.7		40.78
9^5B_2	CAS	2.3331	4.487	148.1	91.9	42.2	13.4	1.59	45.54
	icMRCISD	2.2876	4.325	141.9	124.4	48.9	27.3	1.77	51.65
	icMRCISD+Q				140.8	56.5	38.2		52.35
10^1B_2	CAS	2.2049	3.752	116.6	78.1	28.4	0.4	4.40	59.32
	icMRCISD	2.1769	3.659	114.4	118.9	43.5	21.8	4.14	57.12
	icMRCISD+Q				136.9	52.6	34.3		56.20
11^7A_1	CAS	2.4382	4.625	143.1	78.8	29.1	0.3	2.32	58.62
	MRCISD	2.4679	4.245	118.6	107.3	31.9	10.2	3.72	68.69
	MRCISD+Q				116.8	32.5	14.2		76.35
$12^7\Pi_u$[e]	CAS	2.4445	4.889	180.0	71.6	21.9		0.00	65.84
	MRCISD	2.4032	4.806	180.0	99.0	23.6	1.9	0.00	77.00
	MRCISD+Q				114.5	30.2	11.9		78.65
$12^7B_{1,L}$	CAS	2.4515	4.424	128.9	69.1	19.4		3.32	68.34
	MRCISD	2.3939	4.317	128.7	94.8	19.4		2.84	81.21
	MRCISD+Q				110.4	26.1	7.8		82.72
13^7A_2	CAS	2.4549	4.411	127.9	69.0	19.3		3.44	68.47
	MRCISD	2.4007	4.312	127.8	94.3	18.8		2.97	81.76
	MRCISD+Q				109.7	25.4	7.0		83.47
$14^7\Sigma^-$	CAS	2.4495	4.899	180.0	64.0	14.4		0.00	73.39

ChemPhysChem

Research Article
doi.org/10.1002/cphc.202300365

**Chemistry
Europe**
European Chemical
Societies Publishing

Table 2. continued

State	Methods	R (Mo–S)	R (S–S)	φ (SMoS)	D_e^{1} [a]	D_e^{2} [a]	D_e^{3} [a]	μ	T_e
	MRCISD	2.4003	4.801	180.0	92.8	17.3		0.00	83.24
	MRCISD+Q				108.7	24.4	6.1		84.45
$15^7\Sigma^+$	CAS	2.5400	5.080	180.0	60.1	10.4		0.00	77.36
	MRCISD	2.5046	5.009	180.0	79.8	4.4		0.00	96.20
	MRCISD+Q				93.3	9.1			99.78

[a] $D_e^{1} = - [E(MoS_2) - E(Mo) - 2 \times E(S)]$, $D_e^{2} = -[E(MoS_2) - E(MoS) - E(S)]$, and $D_e^{3} = -[E(MoS_2) - E(Mo) - E(S_2)]$. [b] D_e values with respect to the infinite Mo–S bond distance. With respect to the free atoms $D_e^{1} = 176.0$ kcal/mol (icMRCISD) and 193.1 kcal/mol (icMRCISD+Q). [c] Ref [18], [d] $^5\Pi_u$ components: $^5B_1$ and $^5A_1$. [e] $^7\Pi_u$ components: $^7B_1$ and $^7A_1$.

Table 3. The main electronic Configuration State Functions of MoS_2 at icMRCISD/ AVQZ($-PP)_{Mo}$.

State	CSFS
$\tilde{X}\,^3B_1$	$0.86\,\lvert 1a_1^2 2a_1^2 3a_1^1\ 1b_1^2 2b_1^1\ 1b_2^2 2b_2^2\ 1a_2^2 >$
1^3A_1	$0.85\,\lvert 1a_1^2 2a_1^2 3a_1^1 4a_1^1\ 1b_1^2\ 1b_2^2 2b_2^2\ 1a_2^2 >$
2^1A_1	$0.86\,\lvert 1a_1^2 2a_1^2 3a_1^2\ 1b_1^2\ 1b_2^2 2b_2^2\ 1a_2^2 >$
3^1B_1	$0.87\,\lvert 1a_1^2 2a_1^2 3a_1^1\ 1b_1^2 2b_1^1\ 1b_2^2 2b_2^2\ 1a_2^2 >$
4^3A_2	$0.85\,\lvert 1a_1^2 2a_1^2 3a_1^1\ 1b_1^2\ 1b_2^2 2b_2^2\ 1a_2^2 2a_1^1 >$
$5^5\Pi\ (^5B_1)$ [a]	$0.83\,\lvert 1a_1^2 2a_1^2 3a_1^1 4a_1^1\ 1b_1^2 2b_1^1\ 1b_2^2 2b_2^2\ 1a_2^2 >$
$5^5B_1\ (L)$	$0.86\,\lvert 1a_1^2 2a_1^2 3a_1^1 4a_1^1\ 1b_1^2\ 1b_2^2 2b_2^1\ 1a_2^2 2a_1^1 >$
$5^5\Pi_u\ (^5A_1)$ [a]	$0.83\,\lvert 1a_1^2 2a_1^2 3a_1^1 4a_1^1\ 1b_1^1 2b_1^1\ 1b_2^2 2b_2^2\ 1a_2^2 >$
$5^5A_1\ (L)$	$0.86\,\lvert 1a_1^2 2a_1^2 3a_1^2\ 1b_1^2 2b_1^1\ 1b_2^2 2b_2^1\ 1a_2^2 2a_1^1 >$
6^3B_2	$0.86\,\lvert 1a_1^2 2a_1^2\ 1b_1^1 1b_1^1\ 1b_2^2 2b_2^2\ 1a_2^2 2a_1^1 >$
7^5A_2	$0.85\,\lvert 1a_1^2 2a_1^2 3a_1^1 4a_1^1\ 1b_1^2 2b_1^1\ 1b_2^2 2b_2^1\ 1a_2^2 >$
8^1A_2	$0.85\,\lvert 1a_1^2 2a_1^2 3a_1^1\ 1b_1^2\ 1b_2^2 2b_2^2\ 1a_2^2 2a_1^1 >$
9^5B_2	$0.74\,\lvert 1a_1^2 2a_1^2 3a_1^1 4a_1^1\ 1b_1^2 2b_1^1\ 1b_2^2 2b_2^2\ 1a_2^1 >$
10^1B_2	$0.83\,\lvert 1a_1^2 2a_1^2 3a_1^1\ 1b_1^2\ 1b_2^2 2b_2^2 3b_2^1\ 1a_2^2 >$
11^7A_1	$0.94\,\lvert 1a_1^2 2a_1^2 3a_1^1 4a_1^1\ 1b_1^1 2b_1^1\ 1b_2^2 2b_2^2\ 1a_2^1 2a_1^1 >$
$12^7\Pi_u\ (^7A_{1,L})$ [b]	$0.89\,\lvert 1a_1^2 2a_1^2 3a_1^1 4a_1^1\ 1b_1^1 2b_1^1\ 1b_2^2 2b_2^2\ 1a_2^1 2a_1^1 >$
$12^7B_{1,L}$	$0.70\,\lvert 1a_1^2 2a_1^2 3a_1^1 4a_1^1\ 1b_1^1 2b_1^1\ 1b_2^2 2b_2^2\ 1a_2^2 2a_1^1 >$
13^7A_2	$0.75\,\lvert 1a_1^2 2a_1^2 3a_1^1 4a_1^1\ 1b_1^1 2b_1^1\ 1b_2^2 2b_2^2\ 1a_2^2 2a_1^1 >$
$14^2\Sigma^-\ (^7A_2)$	$0.67\,\lvert 1a_1^2 2a_1^2 3a_1^1 4a_1^1\ 1b_1^2 2b_1^1\ 1b_2^2 2b_2^1\ 1a_2^1 2a_1^1 >$
$15^7\Sigma^+\ (^7B_2)$	$0.94\,\lvert 1a_1^2 2a_1^2 3a_1^1\ 1b_1^1 2b_1^1\ 1b_2^2 2b_2^2 3b_2^1\ 1a_2^1 2a_1^1 >$

[a] $5^5\Pi_u$ components: $^5B_1$ and $^5A_1$.[b] $12^7\Pi_u$ components: $^7B_1$ and $^7A_1$.

Figure 1. PEC for the ground state $\tilde{X}^3B_1$ of MoS_2 with the angle equal to 115.94° (minimized geometry) at the MRCI/AVQZ-PP level of theory.

value;[20] i.e., the D_0 calculated (experimental) values are 91.48 (90.67 ± 0.09) kcal/mol. While, for the S_2 ($X^3\Sigma_g^-$) molecule, the CCSD(T)/wCV5Z[38] calculated (experimental)[39] dissociation energy is 102.5(102.9) kcal/mol.

The PES of the $\tilde{X}^3B_1$ state is plotted in Figure 2. For an SMoS angle equal to 180 degrees, the minimum structure of the linear SMoS is located 26.7 kcal/mol higher in energy than the minimum structure of the ground state, the Mo–S distance is elongated by about 0.02 Å, i.e., at 2.158 Å, while the Mo–S bond distance in the $\tilde{X}^3B_1$ minimum is 2.133 Å.

Two double bonds are formed between the metal and each sulfur atom, i.e., $a_1^2 a_1^2 b_2^2 a_2^2$, see Scheme 2. The bonding molecular

Figure 2. PES E(R, theta) of ground state $\tilde{X}^3B_1$ of MoS_2 at the MRCI/AVQZ-PP level of theory.

energy D_e^3 with respect to ground states of the Mo (^7S) + S_2 ($X^3\Sigma_g^-$), is 90.5 kcal/mol. It is expected the D_e^2 value to be larger than the D_e^3 value, since the calculated D_e value of MoS($X^5\Pi$) is smaller than the D_e value of S_2 ($X^3\Sigma_g^-$), by about 10 kcal/mol. The MoS($X^5\Pi$) D_e value was calculated recently by our group at 92.01 kcal/mol (complete basis set limit of the C-RCCSD[T]/aug-cc-pwCVxZ($-PP)_{Mo}$ method, where the correlation of the core orbitals 4s4p of Mo and 2s2p of S have also been calculated).[20] This value is in excellent agreement with our experimental
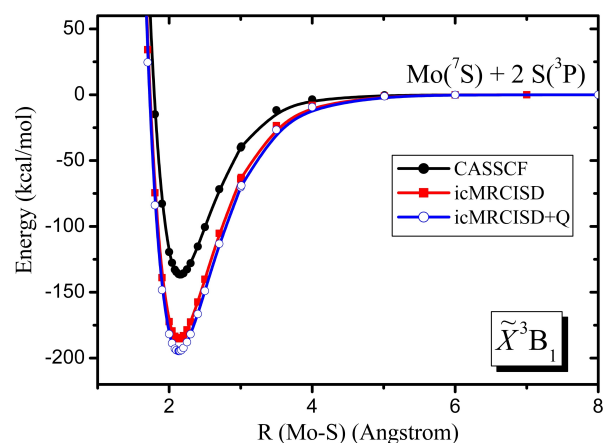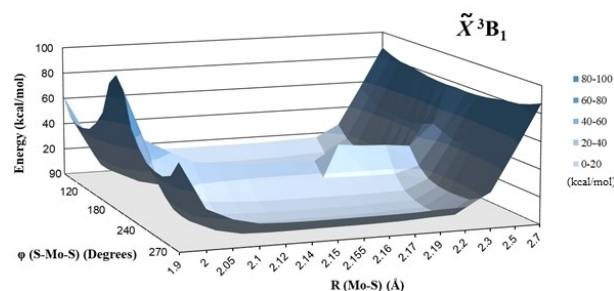
Table 4. Mulliken Population Analysis of Mo and S_2 and Mo's charge, q_{Mo}, at CAS/VTZ$(-PP)_{Mo}$ level.

State	Mulliken population analysis Mo/S_2	q_{Mo}
$\tilde{X}\ ^3B_1$	$5s^{0.66}5p_z^{0.13}5p_x^{0.13}5p_y^{0.19}4d_{z^2}^{0.76}4d_{x^2-y^2}^{1.04}4d_{xz}^{1.09}4d_{yz}^{0.92}4d_{xy}^{0.80}/3s(a_1)^{1.86}3s(b_2)^{1.91}3p_z(a_1)^{1.20}3p_z(b_2)^{1.77}3p_x(b_1)^{1.67}3p_x(a_2)^{1.24}3p_y(a_1)^{1.39}3p_y(b_2)^{1.18}$	0.26
$1\ ^3A_1$	$5s^{0.80}5p_z^{0.25}5p_x^{0.08}5p_y^{0.18}4d_{z^2}^{1.10}4d_{x^2-y^2}^{1.04}4d_{xz}^{0.58}4d_{yz}^{0.86}4d_{xy}^{0.85}/3s(a_1)^{1.86}3s(b_2)^{1.92}3p_z(a_1)^{1.41}3p_z(b_2)^{1.84}3p_x(b_1)^{1.32}3p_x(a_2)^{1.14}3p_y(a_1)^{1.50}3p_y(b_2)^{1.16}$	0.20
$2\ ^1A_1$	$5s^{0.76}5p_z^{0.12}5p_x^{0.09}5p_y^{0.16}4d_{z^2}^{1.16}4d_{x^2-y^2}^{1.43}4d_{xz}^{0.43}4d_{yz}^{0.93}4d_{xy}^{0.73}/3s(a_1)^{1.85}3s(b_2)^{1.91}3p_z(a_1)^{1.19}3p_z(b_2)^{1.81}3p_x(b_1)^{1.45}3p_x(a_2)^{1.27}3p_y(a_1)^{1.46}3p_y(b_2)^{1.12}$	0.12
$3\ ^1B_1$	$5s^{0.55}5p_z^{0.13}5p_x^{0.10}5p_y^{0.18}4d_{z^2}^{0.85}4d_{x^2-y^2}^{0.99}4d_{xz}^{1.18}4d_{yz}^{0.90}4d_{xy}^{0.80}/3s(a_1)^{1.86}3s(b_2)^{1.91}3p_z(a_1)^{1.20}3p_z(b_2)^{1.81}3p_x(b_1)^{1.65}3p_x(a_2)^{1.24}3p_y(a_1)^{1.43}3p_y(b_2)^{1.20}$	0.25
$4\ ^3A_2$	$5s^{0.64}5p_z^{0.08}5p_x^{0.13}5p_y^{0.16}4d_{z^2}^{0.92}4d_{x^2-y^2}^{0.96}4d_{xz}^{0.62}4d_{yz}^{0.93}4d_{xy}^{1.24}/3s(a_1)^{1.87}3s(b_2)^{1.93}3p_z(a_1)^{1.30}3p_z(b_2)^{1.78}3p_x(b_1)^{1.35}3p_x(a_2)^{1.65}3p_y(a_1)^{1.33}3p_y(b_2)^{1.16}$	0.29
$11\ ^7A_1$	$5s^{0.66}5p_z^{0.10}5p_x^{0.03}5p_y^{0.17}4d_{z^2}^{1.02}4d_{x^2-y^2}^{0.98}4d_{xz}^{0.99}4d_{yz}^{0.47}4d_{xy}^{0.99}/3s(a_1)^{1.93}3s(b_2)^{1.92}3p_z(a_1)^{1.73}3p_z(b_2)^{1.83}3p_x(b_1)^{0.98}3p_x(a_2)^{1.00}3p_y(a_1)^{1.61}3p_y(b_2)^{1.54}$	0.51
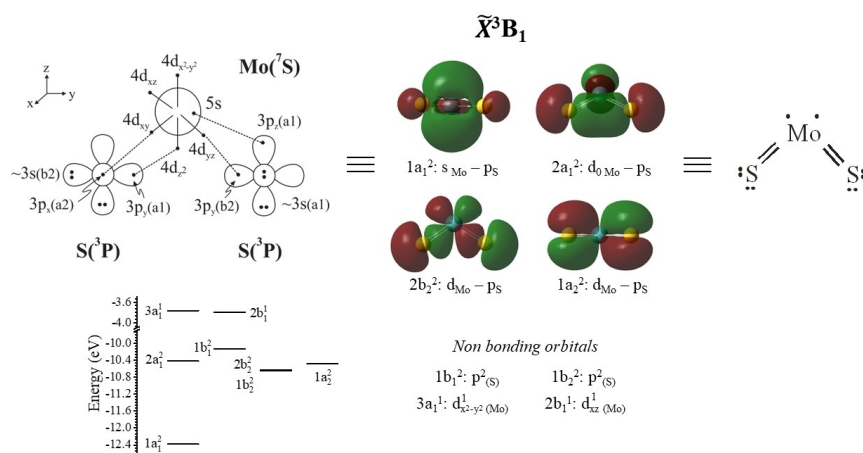
Scheme 2. Chemical bonding of the ground state: vbL diagram, molecular orbitals, vbL bonding, and molecular orbital energies.

orbitals are drawn, and the corresponding valence bond Lewis (vbL) diagram is depicted, Scheme 2. Specifically, there are two a_1^2 bonds, i.e., $5s^1_{[Mo]}-3p_z(a_1)^1_{[S]}$ and $4d_{z^2}^1{}_{[Mo]}-3p_y(a_1)^1_{[S]}$, one b_2^2 bond, i.e., $4d_{yz}^1{}_{[Mo]}-3p_y(b_2)^1_{[S]}$, and one a_2^2 bond, i.e., $4d_{xy}^1-3p_x(a_2)^1$. All three atoms in the $\tilde{X}^3B_1$ state are participating via their atomic ground states, i.e., to Mo $(^7S)+2S$ (^3P). The state has a main CSF with a coefficient of 0.86 showing that the state has a multireference character, see Table 3.

The AVQZ$(-PP)$ dipole moment of the X state is 4.10 Debye and its plot with respect to the Mo–S distance is depicted in Figure 3. The μ value is increased up to 3.0 Å as the Mo–S distances increase; its largest value is 5.34 Debye at 3.0 Å, i.e., it is 1.2 Debye larger than the μ value in the minimum. The increase of the μ value occurs because the Mo atom presents the largest charge at 3.0 Å. It should be noted that μ values using the VQZ$(-PP)$ and VTZ$(-PP)$ are the same, they differ only less than ± 0.04 Debye. However, while the dipole moment is basis set independent, this is not the case for the Mulliken charges. The Mulliken CASSCF charge of the Mo in the minimum is $+0.26$ using the VTZ$(-PP)$ basis set, -0.05 using the VQZ$(-PP)$, and -0.69 using the AVQZ$(-PP)$!! Note that the corresponding NPA CASSCF/VTZ$(-PP)$ charge of Mo in the minimum is $+0.31$ in agreement with the corresponding Mulliken charge with the same VTZ$(-PP)$ basis set. Finally, it should be noted that the Mo Mulliken charges in all three basis sets present an increase as the Mo–S distance increases up to 3.0 Å. At 3.0 Å, all basis sets present positive charges on Mo from $+0.41$[AVQZ$(-PP)$] to $+0.56$[VTZ$(-PP)$] and then the Mo's
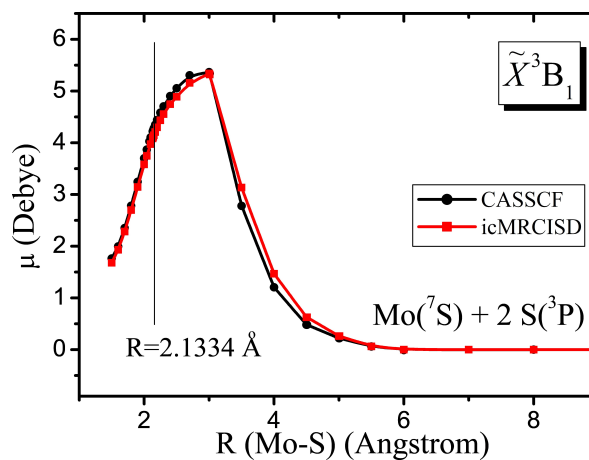

Figure 3. Dipole moments of the X $^3B_1$ state of MoS_2 with respect to the R (Mo–S) distance retaining the S–Mo–S angle to $115.94°$ (minimum structure of the $^5\Pi$ state) at the CASSCF and icMRCISD/AVQZ$(-PP)_{Mo}$ level of theory. The vertical line depicts the Mo–S equilibrium bond distance.

positive charge decreases and at 6 Å where the Mo–S bonds have broken, it becomes zero.

First Excited State, $1\ ^3A_1$

The $^3A_1$ is lying 11 kcal/mol higher than the ground $\tilde{X}^3B_1$ state. Its Mo–S bond distances are 2.139 Å and the (S–Mo–S) angle is

ChemPhysChem

Research Article
doi.org/10.1002/cphc.202300365

Chemistry Europe
European Chemical
Societies Publishing

117.3°. As in the case of the ground state, two double bonds are formed between Mo and the S atoms, i.e., $a_1^2 b_1^2 b_2^2 a_2^2$. The two states differ to the type of the single occupied d orbitals, i.e., $4d_{x^2-y^2}^1$ and $4d_{xz}^1$ in the $\tilde{X}^3B_1$ state and $4d_{x^2-y^2}^1$ and $4d_{z^2}^1$ in the 1^3A_1 state. The a_1^2 bond is formed between the $5s^1$ of Mo and the $3p_y(a_1)^1$ of S; the second one, b_1^2, is formed between the $4d_{xz}^1$ of Mo atom and the $3p_x(b_1)^1$ of S; the b_2^2 bond between the $4d_{yz}^1$ of Mo atom and the $3p_y(b_2)^1$ of S; while the fourth one, a_2^2, is formed between the $4d_{xy}^1$ and $3p_x(a_2)^1$ orbitals. It should be noted that there is strong hybridization $5s5p_z$, $4d_{xz}5p_x$, and $4d_{yz}5p_y$ in the Mo atom. Additional charge is transferred to the 5p orbitals of the Mo atom from the double occupied 3s or 3p orbitals of S, ending up with an electron charge in the Mo's 5p orbitals up to 0.25 e$^-$.

The icMRCISD+Q dissociation energy with respect to the atomic ground state products is 181.9 kcal/mol and with respect to $MoS(X^5\Pi) + S(^3P)$ is 97.6 kcal/mol. The dipole moment of the 1^3A_1 state is 2.33 Debye, i.e., it is almost half of the corresponding value of the $\tilde{X}^3B_1$ state. The Mo atom has the similar electron charge in both states with slightly larger positive charge in the ground than in the 1^3A_1 state. This difference of course may affect the dipole moments, however the difference in the value of the dipole moments may be attributed to the different single occupied orbitals, double 3p orbitals of S, as also as to the different symmetry of the bonding. In $\tilde{X}^3B_1$, the bonding is $a_1^2 \mathbf{a_1^2} b_2^2 a_2^2$, the single occupied orbitals are the $4d_{x^2-y^2}^1$ and $\mathbf{4d_{xz}^1}$ orbitals and the double $3p^2$ occupied orbitals of sulfur are $\mathbf{3p_x^2(b_1)}$ and $3p_z^2$ (b_2). In 1^3A_1, the bonding is $a_1^2 \mathbf{b_1^2} b_2^2 a_2^2$, the single occupied orbitals are the $4d_{x^2-y^2}^1$ and $\mathbf{4d_{z^2}^1}$ orbitals, and the double $3p^2$ occupied orbitals of sulfur are $\mathbf{3p_z^2(a_1)}$ and $3p_z^2(b_2)$. For the dipole moment values, what matters is where the centroid of the electronic distribution in an orbital is located relative to the centroid of the remaining charges in the molecule. Thus, it seems that the centroid of the a_1^2 bonding electron distribution lies on the z-axis, but farther away from the Mo atom than the centroid of the b_1^2 bonding electron distribution. Thus, the dipole moment in the 1^3A_1 state still points in the direction away from the Mo atom and toward the S atoms but has a smaller magnitude than in the ground $\tilde{X}^3B_1$ state.

4^3A_2 and 6^3B_2 States

The 4^3A_2 and 6^3B_2 states have two double bonds between Mo and S atoms as in the $\tilde{X}^3B_1$ and 1^3A_1. Their dissociation energies to the atomic state products are 165.8 kcal/mol and 154.9 kcal/mol, respectively. The bonding in both states is $a_1^2 a_1^2 b_1^2 b_2^2$, while their single occupied d electrons are the $4d_{z^2}$ and $4d_{xy}$ orbitals in 4^3A_2 and the $4d_{xz}$ and $4d_{xy}$ orbitals in 6^3B_2. Their dipole moment values are 5.63 Debye and 5.54 Debye, i.e., they present the largest calculated μ values. These two states and the $\tilde{X}^3B_1$ state have two a_1^2 bonds, i.e., bonds which are totally symmetric, they correspond to A_1 irreducible representation and thus they significantly contribute to the charge separation along z axis, and this causes the increased dipole moment value compared to the μ value of the 1^3A_1 state, see discussion above.

Thus, in all four calculated triplet states, the Mo atom forms double bonds with each of the S atoms. The Mo–S bond distances are similar, and they range from 2.133 Å to 2.171 Å. The SMoS angles are similar and range from 104.2 degree to 117.3 degrees. However, it is of interest that while their bonding is similar, the 6^3B_2 state is lying 39.0 kcal/mol above the $\tilde{X}^3B_1$ state.

2^1A_1 and 3^1B_1 States

The first low-lying singlet states present similar geometry and the shortest Mo–S bond lengths, 2.108 Å (2^1A_1) and 2.128 Å (3^1B_1), see Table 2. Both states are characterized by a severe hybridization of the 5s with $5p_z$, $4d_{x^2-y^2}$ and $4d_{z^2}$ of the Mo atom Additionally, a hybridization of the linear combinations $3p_y(a_1)$ and $3p_z(a_1)$ of the S_2 system is also observed. Due to the spin multiplicity of the state, the Mo atom is excited in the ^5D ($5 s^2 4d^4$) atomic or in the ^5G ($5 s^1 4d^5(^4G)$) atomic state. Note that the $^1B_1$ state is an open singlet state, see Table 2. In both states, the Mo atom forms two bonds with each S (^3P) atom. The $a_1^2 b_1^2 b_2^2 a_2^2$ chemical bonding and corresponding molecular orbitals of the 2^1A_1 state are plotted in Scheme 3.

$5^5\Pi_u$: $^5A_1$ and $^5B_1$ States

The lowest quintet state is the $5^5\Pi$ linear state, which is located 37.5 kcal/mol above the ground $\tilde{X}^3B_1$ state. Its Mo–S bond distance is 2.257 Å and it presents a dissociation energy with
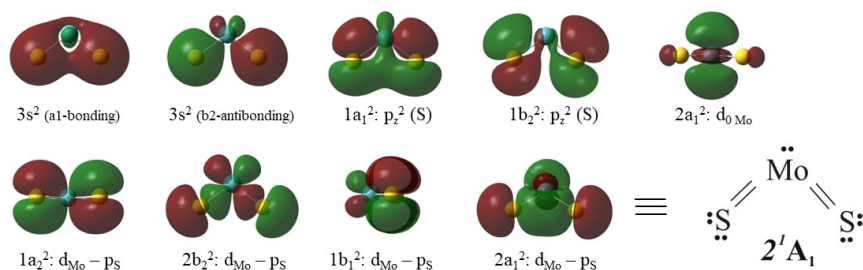
Scheme 3. Chemical bonding of the 2^1A_1 state: vbL diagram and molecular orbitals.

respect to the atomic ground state products of 155.6 kcal/mol, see Table 2. As the molecule bends, the $5^5\Pi_u$ state splits to $^5A_1$ and $^5B_1$. In other words, the $^5A_1$ and $^5B_1$ states are degenerate in their minimum and they are both linear. The $5^5\Pi_u$ is an example of the Renner–Teller effect and the splitting of the $5^5\Pi$ with respect to the SMoS angle is depicted in Figure 4. Both $^5A_1$ and $^5B_1$ configurations present a local minimum (L) at about 90 degrees, due to avoided crossing with higher energy states, see Figure 4. The PES around the local minima are depicted in Figure 5. The SMoS angle at the local minima is 94.3 degrees for the $^5A_1$ state and 88.1 degrees for the $^5B_1$ state. The corresponding Mo—S bond distances are 2.239 Å ($^5A_1$) and 2.238 Å ($^5B_1$). Finally, the local minima are 11.3 kcal/mol and 17.9 kcal/mol higher in energy than the linear $5^5\Pi$ state and the energy barrier is very small, i.e., 0.6 kcal/mol for the $^5A_1$ state and 1.0 kcal/mol for the $^5B_1$ state, see Figures 4 and 5.

Regarding the bonding in the linear $5^5\Pi_u$ state (energetically degenerate $^5A_1$ and $^5B_1$ states) the Mo atom forms a double bond with one of the two S atoms and a single bond with the other one. Note that both configurations are present, and the Mo—S bonds are strictly equivalent, see Scheme 4. The chemical bond of the $5^5\Pi_u$ state is described in C_{2v} symmetry, where the z-axis is vertical to the axis of the molecule as in the cases of the bent states for reason of comparison, and in $D_{\infty h}$ symmetry, which is the real symmetry of this state. Thus, in C_{2v} symmetry, when the z-axis is vertical to the axis of the molecule, the bond is labeled as $a_1^2 b_2^2 a_2^2$. The a_1^2 bond corresponds to a 5
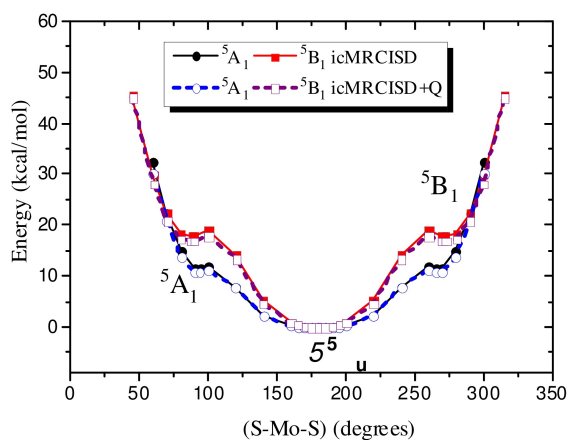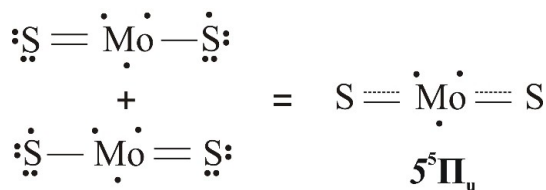
$s^1_{[Mo]}$—$3p_y(a_1)^1_{[S]}$ bond, the b_2^2 corresponds to a $4d^1_{yz[Mo]}$—$3p_z(b_2)^1_{[S]}$ bond and the a_2^2 is a $4d^1_{xy[Mo]}$—$3p_x(a_2)^1_{[S]}$ bond. Both degenerate $^5A_1$ and $^5B_1$ states have the same single occupied Mo's d electrons, i.e., $4d^1_{z^2}4d^1_{x^2-y^2}4d^1_{xz}$, but they differ to which p electrons of S are single or double occupied, i.e., $3p_z(a_1)^1 3p_x(b_1)^2$ in $^5B_1$ and $3p_z(a_1)^2 3p_x(b_1)^1$ in $^5A_1$. In $D_{\infty h}$ symmetry, the bonding orbitals and the four one electron orbitals of the $5^5\Pi$ state are labeled as $\sigma_u^2\pi_g^2\pi_u^2\pi_u^1\sigma_g^1\delta_g^1\delta_g^1$.

Finally, the bonding of local minima of the $^5A_1$ and $^5B_1$ states consists of a double bond between the Mo atom and one S atom and a single bond between the Mo with the other S atom. The single occupied orbitals are $4d^1_{z^2}4d^1_{x^2-y^2}4d^1_{xy[Mo]}\ 3p_y(b_2)^1_{[S]}$ in the local minimum of the $^5B_1$ state and $4d^1_{x^2-y^2}4d^1_{xz}4d^1_{xy[Mo]}\ 3p_y(b_2)^1_{[S]}$ in the local minimum of the $^5A_1$ state, see Table 3. To sum up, in the global minimum ($5^5\Pi$) of the degenerate $^5A_1$ and $^5B_1$ states and in their local minima, where the degeneracy is lifted, all atoms are in their ground states, but they differ to which molecular orbitals form the bonding, i.e., $a_1^2 b_2^2 a_2^2$ in $5^5\Pi$, $a_1^2 b_1^2 b_2^2$ in $^5B_{1[L]}$, and $a_1^2 a_1^2 b_2^2$ in $^5A_{1[L]}$.

Finally, the dipole moment of the lowest energy quintet states with respect to the SMoS angle are plotted in Figure 6. The dipole moment of the local minima are 5.30 Debye ($^5A_1$) and 4.74 Debye ($^5B_1$) states, and as the SMoS *angle decreases*, the μ values further are increased, *see* Figure 6.

7^5A_2, 8^1A_2, 9^5B_2, and 10^1B_2 States

The 8^1A_2 and 10^1B_2 states are open shell singlet states, their Mo—S bond distances are 2.149 and 2.177 Å and their SMoS angles are 104.1 degrees and 114.4 degrees, respectively. Their dissociation energy with respect to the ground atomic state products are 152.3 and 136.9 kcal/mol. Finally, comparing the four calculated singlet states, 2^1A_1, 3^1B_1, 8^1A_2, and 10^1B_2, it is found that their Mo—S bond lengths are increased as the singlet states are higher in energy, i.e., 2.108 Å (2^1A_1), 2.128 Å (3^1B_1), 2.149 Å (8^1A_2), and 2.177 Å (10^1B_2). Finally, their dipole moments range from 4.14 Debye (10^1B_2) to 5.28 Debye (8^1A_2).

The two quintet states, 7^5A_2 and 9^5B_2, present larger Mo—S bond distances than the singlet or triplet states, which is reasonable since the Mo forms a single bond with one S atom and double bond with the other one. Note that the molecular picture (Scheme 1) and its mirror image are present, so the bonding of the two S atoms are strictly equivalent. The calculated Mo—S bond lengths are 2.208 and 2.288 Å and the SMoS angles are 124.8 degrees and 141.9 degrees, respectively. Thus, they present the largest SMoS angles among all bent states. Their dissociation energy with respect to the ground atomic state products are 154.3 and 140.8 kcal/mol. Finally, they present the smallest dipole moments among the calculated states, i.e., 1.78 Debye (7^5A_2) and 1.77 Debye (8^5B_2).

Septet States

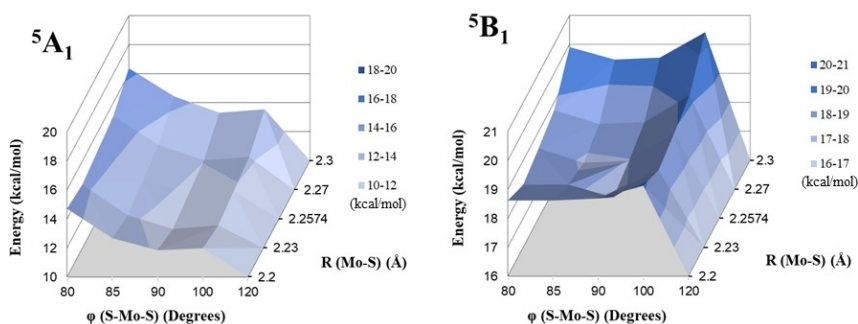These states are important even though they are lying more than 70 kcal/mol above the ground state, because they are

Figure 4. Splitting of the MoS$_2$ (linear) $5^5\Pi_u$ state as a function of the φ (S—Mo—S) angle; PEC of the $^5A_1$ and $^5B_1$ states of MoS$_2$ retaining the Mo—S distance to the minimum bond length of the $5^5\Pi$ state (2.257 Å) at the icMRCI(+Q)/AVQZ($-$PP)$_{Mo}$ level of theory; icMRCISD: solid line icMRCISD+Q: dotted line.

Scheme 4. Chemical bonding of the $5^5\Pi_u$ state. (There is one unpaired electron on one S atom.)

Figure 5. PES of $^5A_1$ and $^5B_1$ states of MoS_2 at the MRCI/AVQZ-PP level of theory.
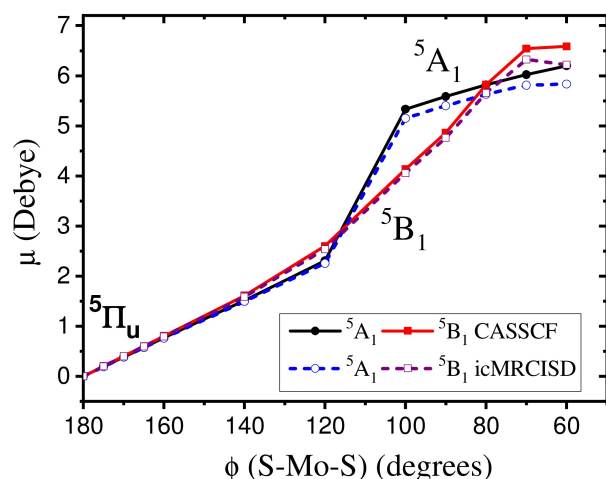

Figure 6. Dipole moments of the $^5A_1$ and $^5B_1$ states of MoS_2 with respect to the φ (S–Mo–S) angle retaining the Mo–S distance to the minimum bond length of the $^5\Pi_u$ state (2.257 Å) at the CASSCF and icMRCISD/AVQZ(−PP)$_{Mo}$ level of theory; CASSCF: solid line icMRCISD: dotted line.

Figure 7. Relative energy differences of the calculated states at TPSSh, CASSCF, icMRCISD, and icMRCISD+Q/AVQZ(−PP)$_{Mo}$ levels of theory.

involved in 2D MoS_2, in solid MoS_2 and in complexes, see below. The lowest septet state is the $11\,^7A_1$. In all septet states, the Mo atom forms one bond with each S atom, see Scheme 1. The calculated states differ in which 4d electrons of Mo and 3p of the S atoms are paired. The Mo–S bond distances are elongated up to 0.4 Å with respect to the triplets or singlets states, where two double bonds are formed. The SMoS angle in the bent structures is about 120 degrees. The dipole moments range from 2.84 Debye to 3.72 Debye. In the $12\,^7\Pi_u$ state, when the MoS_2 molecule bends, the $12\,^7\Pi_u$ state splits to $^7B_1$ and $^7A_1$. The global minimum of the $^7A_1$ state is at the SMoS angle of 118.6 degrees, while the $^7B_1$ state has a local minimum at 128.7 degrees. In DFT level of theory only the $^7B_1$ state has been calculated. The DFT data are in good agreement with the multireference ones.

To sum up, the relative energy (T_e) ordering of the calculated states is depicted in Figure 7. It is found that for the triplet and the quintet states, the T_e values are larger in the icMRCISD and icMRCISD+Q levels comparing to the CASSCF values, on the contrary in the singlet states, the T_e values are smaller or the same. CASSCF calculates static correlation, but not dynamical. In the MoS_2 molecule, the failure in the inclusion of the dynamical correlation at CASSCF is observed in the
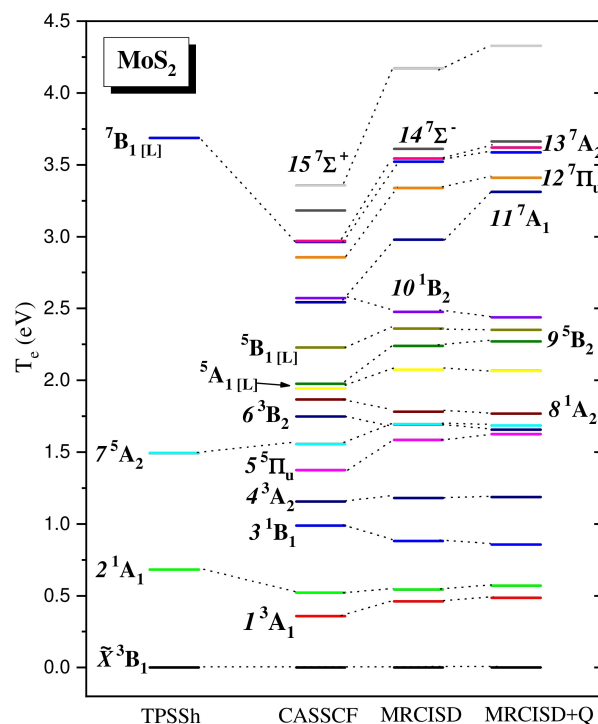
calculation of the dissociation energy. Comparing the CASSCF Mo–S bond distances with the icMRCISD ones, the last one values are 2 to 5% shorter than the CASSCF values. On the contrary, the CASSCF D_e values with respect to the atomic ground states products are significantly underestimated. The icMRCISD values are larger about 28–52% than the CASSCF D_e values, while the icMRCISD+Q values are 41–75% larger than the CASSCF values. Moreover, the icMRCISD+Q D_e values are 5–15% larger than the icMRCISD values; a rather larger increase in D_e values is observed which results from the fact that 14 electrons are correlated and the single and double excitations of the icMRCISD are not enough. Finally, regarding the TPSSh/AVQZ(−PP)$_{Mo}$ methodology, it predicts very well the calculated $\tilde{X}^3B_1$, $2\,^1A_1$, and $7\,^5A_2$ states comparing to our icMRCISD+Q results since it includes part of dynamical and static correlation. Thus, for large molecular systems included Mo–S bonds, the

ChemPhysChem

Research Article
doi.org/10.1002/cphc.202300365

Chemistry Europe
European Chemical
Societies Publishing

DFT methodology using the TPSSh functional can be regarded as a good method.

MoS$_2$ Building Block in 2D MoS$_2$ Surfaces

The MoS$_2$ is the building block in layered MoS$_2$ materials known for its various shapes and morphologies.[40,41] The MoS$_2$ exists in three polymorphic crystalline structures: 1T (tetragonal), 2H (hexagonal), and 3R (rhombohedral), while in the case of 2D material the 3R and 1T structures are the same.[40,41] Moreover, MoS$_2$ layered materials are observed to exhibit other morphologies, such as planar[42] and vertically aligned nanosheets,[43] nanotubes,[44] nanoflowers,[45] nanowires,[46] and nanoplatelets,[47] where the layers are stacked one on top of another and the bonds between the layers are very weak. The observed variety of forms are controlled by selecting the synthesis routes, while the 2D-MoS$_2$ properties can be tuned to develop high performance devices for various applications.[42–57] It is interesting that while, in both 2H and 1T morphologies, each Mo is surrounded by six S atoms, forming single covalent Mo—S bonds, the 2H phase has a trigonal prismatic coordination and the 1T phase have an octahedral one. This small difference in coordination results in being the 2H phase a relative stable and semiconducting phase of poor conductivity, while the 1T′ phase is a metallic one, but unstable at ambient conditions.[48–50]

The 2H, 1T, and 1T′ phases of the 2D MoS$_2$ layer were calculated at DFT-D3(PBE-D3) level of theory, see Figure 8. Both experimentally and theoretically the 2H phase is found as the most stable one.[48] It is more stable than 1T by 0.63 eV per formula unit and by 0.59 eV than 1T′. In 3D material the 2H phase is more stable than 1T by 0.85 eV.[53] Similar values have been calculated for all Mo-dichalogenides.[58–60] For instance for MoSe$_2$, the 2H phase is the most stable phase, and the 1T is higher in energy by 0.68 eV per formula unit and the 1T′ phase

by 0.34 eV.[60] In the 2H phase, all Mo—S distances are calculated at 2.402 Å and all SMoS angles are 82.1 degrees. On the contrary, in the 1T and 1T′ phases, the Mo—S bond distances range from 2.387 to 2.475 Å and the SMoS angles range from 81.0 to 110.8, see Table 5 and Figure 8. Both 1T and 1T′ phases have octahedral coordination and in the 1T′ phase the Peierls distortion dimerization pattern is observed, see Figure 8. In each octahedral structure of 1T or 1T′, all Mo—S are not equivalent, three Mo—S bonds are 2.39 Å and three about 2.46 Å, while there are building blocks of MoS$_2$ with SMoS angles equals to about 110 degrees and MoS bonds of 2.39 Å.

In 2D-MoS$_2$ and MoS$_2$ solid, the Mo—S bonds are single covalent bonds. In the triatomic MoS$_2$ molecule, the ground and the low-lying in-energy triplet and singlet states forms double Mo—S bonds. However, in the bent septet states, single bonds are formed, with bond distance that ranges from 2.39 to 2.47, i.e., the same Mo—S bond distances with the calculated values in the 2D MoS$_2$, see above. Note that the Mo—S distances in various polymorphs of Molybdenum sulfide are similar, i.e., 2.38–2.59 Å,[20,56] while in complexes and enzymes are about 2.35 Å.[57] For instance, in nitrogenase, which is a complex enzyme that catalyzes the formation of ammonia, the Mo—S bond distances ranges from 2.31 to 2.35 Å.[61] It should be noted that in complexes the Mo—S bond distances are shorter that the triatomic, because in complexes, the Mo atoms are more positively charged than in triatomic and the bonds have a ionic character, while in triatomic MoS$_2$ which is neutral, the bonds are mainly covalent. The icMRCISD energy difference among the lowest in energy $^7A_1$ and $^7B_1$ is 12.5 kcal/mol (~0.54 eV), similar to the relative energy difference per formula unit in the different phases, 2H, 1T, and 1T′. Furthermore, it is worth noting that the septet states of the diatomic MoS, which present half or a single bonds, have bond distances that range from 2.36 to 2.52 Å.[20] The lowest septet state, $^7\Pi$, has a dissociation energy of 2.66 eV, only 0.3 eV larger than the formation of the S vacancy of solid MoS$_2$, 2.35 eV in S-rich conditions.[55]

The calculated septet states of MoS$_2$ lie close in energy, i.e., the bent septet states differ in energy less than 10 kcal/mol, and as a result, all can be involved in the 2D material. Thus, the different septet states of diatomic MoS and triatomic MoS$_2$ molecules that are included in the 2D material are responsible for the variety of the various phases and polymorphs of molybdenum sulfide. Note that in the septet states, the molybdenum presents an sd^5 hybridization and it has the ability

Table 5. Mo—S distances in Å, φ (S—Mo—S) in degrees, and relative total energy per formula unit ($\Delta E_i = E_{tot\ i} - E_{tot\ 2H}$) in kcal/mol, in the 2H, 1T, and 1T′ phases of 2D-MoS$_2$.

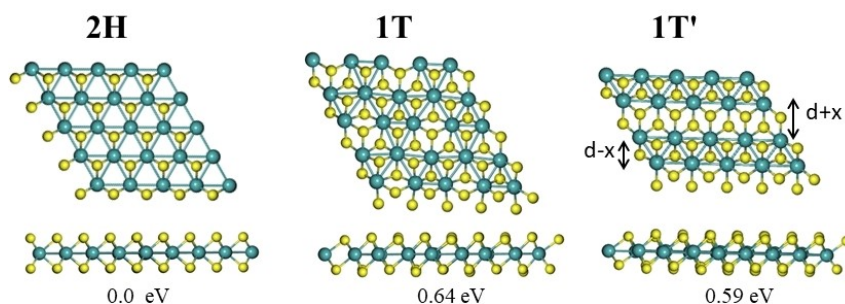| Phase	Mo—S	SMoS	ΔE_i
2H	2.402	82.1	0.0
1T	2.387–2.461	82.9–109.3	14.8
1T′	2.391–2.475	82.1–110.8	13.5

Figure 8. 2D-MoS$_2$ structures in the 2H, 1T, and 1T′ phases via two points of view; relative total energy per formula unit.

ChemPhysChem

Research Article
doi.org/10.1002/cphc.202300365

Chemistry Europe
European Chemical
Societies Publishing

to form six bonds. The study of the triatomic (and diatomic) molecules can provide useful information to understand the solid and 2D MoS_2 as well as molybdenum complexes, while their relation of isolated MoS and MoS_2 species to the relevant material and complexes is far from trivial. In 2D material, the electronic properties have a strong dependence on the structural phase. For instance, the 2H MoS_2 phase is semiconductor, and it presents a tunable bandgap of $\sim$1.2–1.9 eV which depends on the number of layers.[51] Additionally, molybdenum sulfide compounds can be used as an efficient catalyst[54] and their structure and properties are very important. Finally, for some morphologies such as 2D 1T'-MoS_2, little is known probably because of the limited phase uniformity ($<$ 80%) and lateral size (usually $<$ 1 μm) in produced materials.[53] Thus, the present data may open a new approach to explore the properties of 2D metastable polymorphic materials.

Conclusions and Summary

In the present study, sixteen low-lying excited states of MoS_2 are studied via DFT and accurate multi reference configuration interaction methodologies. Geometries, dissociation energies, and dipole moments are calculated. The chemical bonds connecting the atoms are analyzed, while potential energy curves (PEC) and potential energy surfaces are provided. Finally, the connection of the chemical bonding of the isolated MoS_2 molecule to the relevant solid, MoS_2, is emphasized to light a shed on the functionality of the MoS_2 complexes or materials.

All calculated states consist of atoms in their atomic ground states, except singlets, where the Mo atom is excited. In the triplet and the singlet states, the Mo atom forms double bonds with each S atom, i.e., Mo forms a quadruple bond. In the quintet states, the Mo atom forms a double bond with one S atom and a single bond with the other, while in the septet states, the Mo atom forms single bonds with each S atom. Most of the calculated states are bent with an SMoS angle that ranges from 104.2 degrees ($^3A_2$) to 141.9 degrees ($^5B_2$). Four linear states were calculated, i.e., $5^5\Pi_u$, $12^7\Pi_u$, $14^7\Sigma^-$, and $15^7\Sigma^+$. The $5^5\Pi_u$ state, as the molecule bends, splits into $^5A_1$ and $^5B_1$ states, because of the Renner–Teller effect. The Mo–S bond distances range from 2.109 Å (2^1A_1) to 2.505 Å ($^7\Sigma^+$). Finally, the dipole moments are calculated up to 5.63 Debye (4^3A_2). The smallest values in the bent states are observed in the $^5A_2$ and $^5B_2$ states at about 1.8 Debye.

In the ground state, $X\,^3B_1$, the Mo–S bond distances are calculated at 2.133 Å and the SMoS angle at 115.9°, in very good agreement with the experimental value of 114±3 degrees.[18] The dissociation energy with respect to the atomic ground state products, Mo (^{7}S)+2S (^{3}P), is calculated at 194.7 kcal/mol and the dissociation energy with respect to MoS ($X\,^5\Pi$)+S (^{3}P) is 108.8 kcal at the icMRCISD+Q/AVQZ(−PP)$_{Mo}$ level of theory.

In the ground $\tilde{X}^3B_1$ and the first 1^3A_1 excited states, the Mo atom forms two double bonds with each S atom, $a_1^2 a_1^2 b_2^2 a_2^2$ ($\tilde{X}^3B_1$) and $a_1^2 b_1^2 b_2^2 a_2^2$ (1^3A_1). The states have different dipole moment values, i.e., 4.10 Debye ($\tilde{X}^3B_1$) and 2.33 Debye (1^3A_1). This

difference can be attributed to the difference between a_1^2 and b_1^2 bonds. The centroid of the a_1^2 bonding electron distribution lies on the z-axis, but farther away from the Mo atom than the centroid of the b_1^2 bonding electron distribution. Thus, the dipole moment in the 1^3A_1 state still points in the direction away from the Mo atom and toward the S atoms but it has a smaller magnitude than in the ground $\tilde{X}^3B_1$ state.

The MoS_2 molecule is the building block in layered MoS_2 materials known for its various shapes and morphologies. The 2H, 1T, and 1T' phases of the 2D MoS_2 layer were calculated at DFT-D3(PBE-D3) level of theory. The 2H phase is the most stable phase. It is more stable than 1T by 0.63 eV per formula unit and by 0.59 eV than 1T'. In morphologies the Mo–S bonds are single covalent bonds with bond distances of 2.39-2.48 Å as in the case of the septet states of the triatomic MoS_2. Thus, the building block of the 2D and solid material is the septet states of MoS_2, so as the six unpaired electrons of the triatomic MoS_2 to form additional bonds with the adjacent MoS_2 units. Different bent septet states of the triatomic, which are close lying in energy, are involved in the 2D MoS_2 and in solid. This results in the variety of the material's morphologies.

To sum up, both diatomic MoS and triatomic MoS_2 molecules can provide useful information to understand the solid and 2D MoS_2 as well as molybdenum complexes, while the relation of isolated MoS and MoS_2 species to the relevant materials and complexes is far from trivial. In 2D material, the electronic properties have a strong dependence on the structural phase. The catalytic properties of molybdenum sulfide compounds also depend on their structure, while for some morphologies such as 2D 1T'-MoS_2, little is known. Thus, the present data may open a new approach to explore the properties of 2D metastable polymorphic materials.

Conflict of Interests

The authors declare no conflict of interest.

Data Availability Statement

The data that support the findings of this study are available from the corresponding author upon reasonable request.

[1] M. Chhowalla, G. Amaratunga, *Nature* **2000**, *407*, 164–167.
[2] M. Remskar, A. Mrzel, Z. Skraba, A. Jesih, M. Ceh, J. Demsar, P. Stadelmann, F. Levy, D. Mihailovic, *Science* **2001**, *292*, 479–81.
[3] S. Chen, Y. Pan, *Appl. Surf. Sci.* **2022**, *599*, 154041.
[4] D. Voiry, A. Mohite, M. Chhowalla, *Chem. Soc. Rev.* **2015**, *44*, 2702.
[5] W. Dong, H. Liu, X. Liu, H. Wang, X. Li, L. Tian, *Int. J. Hydrogen Energy* **2021**, *46*, 9360.
[6] S. Chen, Y. Pan, *Int. J. Hydrogen Energy* **2021**, *46*, 21040.
[7] Z. Li, X. Menga, Z. Zhang, *J. Photochem. Photobio. C: Photochem. Rev.* **2018**, *35*, 39–55.
[8] D. Gupta, V. Chauhan, R. Kumar, *In. Chem. Commun.* **2020**, *121*, 108200.
[9] S. Xu, Y. Zhang, F. Xu, C. Chen, Z. Shen, *Comput. Theor. Chem.* **2020**, *1188*, 112935.
[10] M. I. Khan, S. H. Aziz, A. Majid, M. Rizwan, *Phys. E: Low-dim. Syst. Nanostr.* **2021**, *130*, 114692.
[11] H. Wang, Z. Lu, S. Xu, D. Kong, J. J. Cha, G. Zheng, P.-C. Hsu, K. Yan, D. Bradshaw, F. B. Prinz, Y. Cui, *Proc Natl Acad Sci USA* **2013**, *110*, 19701–19706.
[12] Y. Xue, Y. Zhang, Y. Liu, H. Liu, J. Song, J. Sophia, J. Liu, Z. Xu, Q. Xu, Z. Wang, J. Zheng, Y. Liu, S. Li, Qiaoliang Bao, *ACS Nano* **2016**, *10*, 573–580.
[13] G. S. Bang, K. W. Nam, J. Y. Kim, J. Shin, J. W. Choi, S.-Y. Choi, *ACS Appl. Mater. Interfaces* **2014**, *6*, 7084–7089.
[14] B. M. Hoffman, D. Lukoyanov, Z. Y. Yang, D. R. Dean, L. C. Seefeldt, *Chem. Rev.* **2014**, *114*, 4041.
[15] J. Xu, J. Zhang, W. Zhang, C. S. Lee, *Adv. Energy Mater.* **2017**, *7*, 1700571.
[16] L. Xie, *Nanoscale* **2015**, *7*, 18392.
[17] S. Wang, Y. Pan, Y. Wu, Y. Lin, *RSC Adv.* **2018**, *8*, 28693.
[18] B. Liang, L. Andrews, *J. Phys. Chem. A* **2002**, *106*, 6945–6951.
[19] P. Cheng, G. K. Koyanagi, D. K. Bohme, *J. Phys. Chem. A* **2006**, *110*, 2718–2728.
[20] D. Tzeli, I. Karapetsas, D. M. Merriles, J. C. Ewigleben, M. D. Morse, *J. Phys. Chem. A* **2022**, *126*, 1168–1181.
[21] J. Tao, J. P. Perdew, V. N. Staroverov, G. E. Scuseria, *Phys. Rev. Lett.* **2003**, *91*, 146401.
[22] D. E. Woon, T. H. Dunning, *J. Chem. Phys.* **1993**, *98*, 1358.
[23] N. B. Balabanov, K. A. Peterson, *J. Chem. Phys.* **2005**, *123*, 064107.
[24] P.-Å. Malmqvist, B. O. Roos, *Chem. Phys. Lett.* **1989**, *155*, 189.
[25] H.-J. Werner, P. J. Knowles, *J. Chem. Phys.* **1988**, *89*, 5803.
[26] S. R. Langhoff, E. R. Davidson, *Int. J. Quantum Chem.* **1974**, *8*, 61–72.
[27] J. P. Perdew, K. Burke, M. Ernzerhof, *Phys. Rev. Lett.* **1997**, *77*, 3865–3868.
[28] H. Schröder, J. Hühnert, T. Schwabe, *J. Chem. Phys.* **2017**, *146*, 044115.
[29] A. Dal Corso, *Comput. Mater. Sci.* **2014**, *95*, 337–350.
[30] Gaussian 16 (Revision C.01), M. J. Frisch, G. W. Trucks, H. B. Schlegel, G. E. Scuseria, M. A. Robb, J. R. Cheeseman, G. Scalmani, V. Barone, G. A. Petersson, H. Nakatsuji, X. Li, M. Caricato, A. V. Marenich, J. Bloino, B. G. Janesko, R. Gomperts, B. Mennucci, H. P. Hratchian, J. V. Ortiz, A. F. Izmaylov, J. L. Sonnenberg, F. Williams-Young, F. Ding, F. Lipparini, F. Egidi, J. Goings, B. Peng, A. Petrone, T. Henderson, D. Ranasinghe, V. G. Zakrzewski, J. Gao, N. Rega, G. Zheng, W. Liang, M. Hada, M. Ehara, K. Toyota, R. Fukuda, J. Hasegawa, M. Ishida, T. Nakajima, Y. Honda, O. Kitao, H. Nakai, T. Vreven, K. Throssell, J. A. Montgomery Jr, J. E. Peralta, F. Ogliaro, M. J. Bearpark, J. J. Heyd, E. N. Brothers, K. N. Kudin, V. N. Staroverov, T. A. Keith, R. Kobayashi, J. Normand, K. Raghavachari, A. P. Rendell, J. C. Burant, S. S. Iyengar, J. Tomasi, M. Cossi, J. M. Millam, M. Klene, C. Adamo, R. Cammi, J. W. Ochterski, R. L. Martin, K. Morokuma, O. Farkas, J. B. Foresman, D. J. Fox, Inc., Wallingford CT **2016**.
[31] H.-J. Werner, P. J. Knowles, F. R. Manby, J. A. Black, K. Doll, A. Heßelmann, D. Kats, A. Köhn, T. Korona, D. A. Kreplin, Q. Ma, T. F. Miller III, A. Mitrushchenkov, K. A. Peterson, I. Polyak, G. Rauhut, M. Sibaev, MOLPRO 2022.3 is a package of ab initio programs **2022**, *J. Chem. Phys.* **2020**, *152*, 144107.
[32] P. Giannozzi, O. Baseggio, P. Bonfà, D. Brunato, R. Car, I. Carnimeo, C. Cavazzoni, S. de Gironcoli, P. Delugas, F. F. Ruffino, et al., *J. Chem. Phys.* **2020**, *152*, 154105.
[33] F. Bickelhaupt, N. Hommes, C. Guerra, E. Baerends, *Organometallics* **1996**, *15*, 2923–2931.
[34] D. Tzeli, I. Petsalakis, G. Theodorakopoulos, *J. Phys. Chem. A* **2011**, *115*, 11749–11760.
[35] D. Tzeli, S. Raugei, S. S. Xantheas, *J. Chem. Theory Comput.* **2021**, *17*, 6080–6091.
[36] F. Maseras, K. Morokuma, *Chem. Phys. Lett.* **1992**, *195*, 500–504.
[37] C. F. Guerra, J.-W. Handgraaf, E. J. Baerends, F. M. Bickelhaupt, *J. Comput. Chem.* **2004**, *25*, 189–210.
[38] K. A. Peterson, T. H. Dunning Jr, *J. Chem. Phys.* **2002**, *117*, 10548–10560.
[39] K. P. Huber, G. Herzberg, *Molecular Spectra and Molecular Structure IV. Constants of Diatomic Molecules*, Van Nostrand, Princeton, NJ **1979**.
[40] Z. Ji, C. Trickett, X. Pei, O. M. Yaghi, *J. Am. Chem. Soc.* **2018**, *140*, 13618–13622.
[41] R. Canton-Vitoria, N. Tagmatarchis, Y. Sayed-Ahmad-Baraza, C. Ewels, D. Winterauer, T. Batten, A. Brunton, S. Nufer, *Gas Sensing Using Monolayer MoS2, Nanoscale Materials for Warfare Agent Detection. In Nanoscience for Security, NATO Science for Peace and Security Series - A: Chemistry and Biology*, Eds. C. Bittencourt, C. Ewels, E. Llobet, Springer: **2017**, 71–96.
[42] H. Xu, J. Yi, X. She, Q. Liu, L. Song, S. Chen, Y. Yang, Y. Song, R. Vajtai, J. Lou, et al., *Appl. Catal. B* **2018**, *220*, 379–385.
[43] X. P. Chen, G. J. Xing, L. F. Xu, H. Q. Lian, Y. Wang, *Compos. Interfaces* **2020**, 1–10.
[44] J. Chen, N. Kuriyama, H. Yuan, H. T. Takeshita, T. Sakai, *J. Am. Chem. Soc.* **2001**, *123*, 11813–11814.
[45] Z. Hu, L. Wang, K. Zhang, J. Wang, F. Cheng, Z. Tao, J. Chen, *Angew. Chem. Int. Ed.* **2014**, *53*, 12794–12798.
[46] W. J. Li, E. W. Shi, J. M. Ko, Z. Z. Chen, H. Ogino, T. Fukuda, *J. Cryst. Growth* **2003**, *250*, 418–422.
[47] G. Deokar, P. Vancsó, R. Arenal, F. Ravaux, J. Casanova-Cháfer, E. Llobet, A. Makarova, D. Vyalikh, C. Struzzi, P. Lambin, et al. *Adv. Mater. Interfaces* **2017**, *4*, 1–10.
[48] C. Zhang, C. Wang, T. Rabczuk, *Phys. E* **2018**, *103*, 294–299.
[49] F. Wypych, R. Schöllhorn, *J. Chem. Soc. Chem. Commun.* **1992**, 1386–1388.
[50] L. Jiang, S. Zhang, S. A. Kulinich, X. Song, J. Zhu, X. Wang, H. Zeng, *Mater. Res. Lett.* **2015**, *3*, 177–183.
[51] D. Pariari, R. M. Varma, M. N. Nair, P. Zeller, M. Amati, L. Gregoratti, K. K. Nanda, D. D. Sarma, *Appl. Mater. Today* **2020**, *19*, 100544.
[52] X. Guo, G. Yang, J. Zhang, X. Xu, *AIP Adv.* **2015**, *5*, 097174.
[53] J. Peng, Y. Liu, X. Luo, J. Wu, Y. Lin, Y. Guo, J. Zhao, X. Wu, C. Wu, Y. Xie, *Adv. Mater.* **2019**, *31*, 1900568.
[54] Y. Li, A. Yamaguchi, M. Yamamoto, K. Takai, R. Nakamura, *J. Phys. Chem. C* **2017**, *121*, 2154–2164.
[55] D. Liu, Y. Guo, L. Fang, J. Robertson, *J. Appl. Phys. Lett.* **2013**, *103*, 183113.
[56] H. Fukuoka, K. Masuoka, T. Hanaoka, K. Inumaru, *In. Chem.* **2013**, *52*, 7918–7922.
[57] C. M. Cordas, J. J. G. Moura, *Coord. Chem. Rev.* **2019**, *394*, 53–64
[58] Y. Zhang, Y. Kuwahara, K. Mori, C. Louisd, H. Yamashita, *Nanoscale* **2020**, *12*, 11908–11915
[59] K.-A. N. Duerloo, Y. Li, E. J. Reed, *Nat. Commun.* **2014**, *5*, 4214
[60] R. Besse, N. A. M. S. Caturello, C. M. O. Bastos, D. Guedes-Sobrinho, M. P. Lima, G. M. Sipahi, J. L. F. Da Silva, *J. Phys. Chem C* **2018**, *122*, 20483–20488
[61] R. Bjornsson, F. Neese, S. DeBeer, *In. Chem.* **2017**, *56*, 1470–1477

RESEARCH ARTICLE

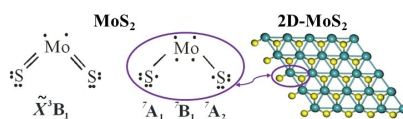**The triatomic MoS₂ molecule** is the building component of solid MoS₂. In this work, the electronic structure and chemical bonding of 16 low-lying states of triatomic MoS₂ are studied. The low-lying septet states of triatomic MoS₂ are found to be involved in the material as a building block, explaining the variety of its morphologies.

M. A. Mermigki, Dr. I. Karapetsas, Prof.Dr. D. Tzeli*

1 – 13

Electronic Structure of the Low-Lying States of the Triatomic MoS₂ Molecule: The Building Block of 2D MoS₂